Available online at www.sciencedirect.com
SCIENCE DIRECT®
Polymer 47 (2006) 5633–5642
polymer
www.elsevier.com/locate/polymer

Nanostructural features of a spider dragline silk as revealed by electron and X-ray diffraction studies

J.E. Trancik [a,b], J.T. Czernuszka [a], F.I. Bell [c], C. Viney [a,c,d,*]

[a] Department of Materials, University of Oxford, Parks Road, Oxford OX1 3PH, UK
[b] Earth Institute, Columbia University, New York, NY 10027, USA
[c] Chemistry, School of Engineering and Physical Sciences, Heriot-Watt University, Edinburgh EH14 4AS, UK
[d] School of Engineering, University of California, Merced, CA 95344, USA

Received 19 December 2004; accepted 8 January 2005
Available online 19 May 2006

Abstract

Transmission electron microscopy (TEM) and X-ray diffraction (XRD) were used to examine the nanostructure of a natural polymer—a spider dragline silk—that has potential applications as an engineering material. The silk studied was collected from the cob-web weaving spider *Latrodectus hesperus.* Single crystal and polycrystalline electron diffraction patterns indicate the presence of crystals with a bimodal size distribution, in the range of 2 nm and 40–120 nm. The chain axis of the smaller crystals is more strictly aligned with the fiber axis than that of the larger crystals. Lattice parameters for the orthogonal unit cell are: $a=9.4$ Å (interchain), $b=7.0$ Å (dipeptide, fiber axis) and $c=10.8$ Å (intersheet). A fine structure in single crystal electron diffraction patterns indicates possible composition-dependent lattice strains. Results of tensile tests of the spider dragline silk are reported, and a simple model is presented linking the observed nanostructural features to the force-elongation response of this material.
© 2006 Elsevier Ltd. All rights reserved.

Keywords: Crystal; Dragline; Electron diffraction

1. Introduction

Silks are natural polymers consisting mostly of the amino acids alanine, serine and glycine, and are produced by arthropods in the classes *Insecta*, *Arachnida* and *Myriapoda* [1,2]. In nature, silk fibers serve a variety of purposes including structural support, protection against the environment, and aid in prey capture.

Native spider dragline silks exhibit high mean strength and toughness in tensile tests conducted at constant strain rate. Although these impressive tensile properties are compromised by creep and stress relaxation [3–5], which in turn are exacerbated by moisture [3,5], there are indications that such limitations can be overcome by post-spinning treatment of the fiber [6]. Continuing attempts to improve the long-term performance of dragline and analogous materials as a route to new engineering materials are motivated by the environmentally sustainable, resource-efficient attributes of silk: while artificial polymers are typically derived from petrochemicals, and require high processing temperatures and/or hazardous solvents, silk proteins are spun into fiber at room temperature from aqueous solutions [7].

Attempts to create artificial silk analogues must take into account not only the chemical components of the native material, but also the microstructural and nanostructural features such as crystal sizes, since these too affect the mechanical properties of a fiber. Biomimetic silk analogs have yet to replicate the mechanical properties of the natural material; however, considerable progress has been reported [8]. In the present work, we set out to characterize nanostructural features of dragline and to relate these to measured tensile properties, in order to help inform the design of silk analogs.

Various types of spider silk have been characterized previously by X-ray diffraction (XRD), NMR and, to a lesser extent, transmission electron microscopy (TEM). XRD characterization of several spider dragline silks has revealed crystals in the range ca. 2–7 nm, with the longer dimensions and polypeptide backbones oriented along the fiber axis [9,10].

* Corresponding author. Address: School of Engineering, University of California at Merced, P.O. Box 2039, Merced, CA 95344, USA. Tel.: +1 209 724 4359; fax: +1 209 724 2912.
E-mail address: cviney@ucmerced.edu (C. Viney).

0032-3861/$ - see front matter © 2006 Elsevier Ltd. All rights reserved.
doi:10.1016/j.polymer.2005.01.110

The crystals have a β-sheet structure and an orthogonal unit cell; they are thought to be primarily composed of polyalanine.

Larger crystals, ranging from 70–500 nm, have been detected in TEM studies of *Nephila clavipes* dragline silk; these have been named non-periodic lattice (NPL) crystals and can be thought of as regions of nearly (but not perfectly) repeated composition and order [11–13]. Their presence has also been inferred from an analysis of XRD patterns obtained from bundles of *N. clavipes* dragline [12]. The model of NPL crystals allows for the presence of small, perfect polyalanine crystals embedded in imperfect areas that contain glycine and some of the other, larger, residues. NMR studies of *Nephila edulis* dragline silk have indicated that, in addition to alanine, glycine residues may be incorporated into β-sheet structures [14]. Moreover, analyses of unit cell scattering amplitudes from 40–120 nm sized crystals in *Latrodectus hesperus* dragline silk have suggested that some of the larger residues are also included in these crystalline structures [15].

TEM of silk polymers is complicated by the rapid degradation of these materials in the electron beam. Degradation of specimens has limited the use of TEM in most previous studies to bright-field imaging (not taking advantage of diffraction and dark-field imaging modes, because of the beam exposure required to obtain data in these modes). Despite the limitations of working with beam-sensitive materials, TEM characterization—and particularly electron diffraction—offers certain benefits over other techniques, since information can be gained from small features in the specimen (ca. 1 nm^2 on the microscope used in the present study) and from isolated crystals in polycrystalline materials. Also, when features are close to the resolution limit of the microscope, their presence is more readily detected in diffraction space than in contrast-limited real space.

Similar, local characterization is not possible using XRD, although X-ray microdiffraction and small-angle scattering techniques using high-brilliance synchrotron radiation have been developed [16].

There are a few other published studies that use TEM diffraction or dark field imaging to characterize individual silk fibers. These focus on: major ampullate silk from the orb-web weaver *N. clavipes* (determining the unit cell dimensions, and demonstrating the NPL characteristics of crystals in this silk) [11,12,17]; cocoon silk from the orb-web weaver *Araneus diadematus* (suggesting that NPL characteristics are not unique to major ampullate silk, and that the crystals in spider cocoon silk are twisted) [18,19]; capture thread from the non-orb-weaving spider *Loxosceles arizonica* (measuring the unit cell parameters, and highlighting the ribbon-like morphology of the fibers) [20]; and cocoon silk from the silkworm *Bombyx mori* (revealing a banded morphology within the fibers, and measuring the mean axial and lateral dimensions of crystallites) [21]. In the present study, we use TEM diffraction to provide the first explicit evidence for the co-existence of populations of small and large crystals in a natural silk.

2. Methods

2.1. Sample collection

The black widow spiders originated in Southern California and were maintained in the laboratory of A. Moore at Claremont College. In order to prevent toxic bites while securing a spider prior to silking, the spiders were anesthetized with CO_2 using the minimum dosage required for immobilization. Silk was collected only after the spider was fully revived. The dragline was reeled from an adult female *L. hesperus*, around a rotating wheel at a linear speed of 4.2 cm/s, taking care to minimize contamination by silk that does not originate in the major ampullate glands. Further details can be found elsewhere [22].

Previous studies have shown that the mechanical properties of major ampullate silk depend on the rate at which the fiber is reeled from the spider [23,24], and that the properties of reeled major ampullate silk are not the same as those of the naturally spun material [25–28]. These differences in mechanical properties must arise from differences in microstructure, evidence of which has been reported for major ampullate silk reeled at different rates [13]. We chose to perform the present study on reeled silk so that samples would have a reproducible history, and in anticipation of the fact that biomimetic silk analogues will experience forced drawing as they are processed into fibers.

2.2. Transmission electron microscopy

As described previously [29], an orienting procedure was developed in which the *L. hesperus* silk was wound around a polyester film (Melinex by Agar Scientific) prior to embedding in resin, in order to align the fibers along a predetermined direction. After washing the silk in two successive baths of ethanol (99.7–100%), the silk was embedded in epoxy resin (TAAB Embedding Resin) and cured at 60 °C for 24 h. (This method draws on that developed by Luft [30] and adapted by Thiel et al. [11].) Precautions were taken to avoid inhalation of resin dust [31]. Sections of 60–90 nm thickness were cut with a diamond knife on a Sorvall Ultra Microtome MT500, and then placed on 3 mm, 400 mesh TEM copper grids. Since it is desirable to avoid modification of the natural micro/nanostructure, most specimens were not stained.

Specimens were examined with a JEOL 4000EX CETEM, equipped with a liquid nitrogen cooling stage and operating at 400 keV. The cooling system was held at −120 °C, the lowest temperature at which ice crystals did not form. To increase the working time before specimen degradation, high accelerating voltages and low beam intensities were used, together with other low-dose imaging techniques [32]. As a result of the low beam intensities required, diffraction patterns and dark field images were not easily resolvable on the screen and often only became visible in the developed negative. Dark field images were obtained by estimating the placement of a diffracted beam and displacing the objective aperture to a position where it was likely to frame the diffracted beam.

In analysis of TEM diffraction patterns, the reflection spacings were measured both visually from magnified negatives, and digitally, in order to verify the peak position of the radially-averaged intensity. The camera length was calibrated using a gold standard. To determine the unit cell dimensions and index the diffraction patterns, the intersheet distance was treated as an unknown variable and refined iteratively, while the interchain and dipeptide spacings in the orthogonal unit cell were set equal to the values obtained from other silks [33].

Crystal sizes were determined from the diffracted beam broadening (along the radial direction), using the Scherrer formula [34]

$$t = \frac{(0.9\lambda)}{(B\cos\theta_B)}$$

where t = crystal diameter, λ = electron wavelength, B = broadening of reflection (an angular width, in terms of 2θ), and θ_B = Bragg angle.

Smaller crystal sizes produce diffuse reflections while larger ones lead to more distinct spots. The broadening was measured at full-width half maximum (FWHM) for reflections on digitized images, where the radial and circumferential directions on the diffraction pattern had been plotted along the vertical and horizontal axes, respectively. Background was subtracted using areas free of reflections.

Negatives were digitized using a Hewlett Packard HP Scanjet 6100C/T. The brightness/contrast of scanned images was modified as needed to preserve relevant features upon reproduction. Any changes in brightness/contrast were applied to the entire negative—specific areas of images were not selectively enhanced. However, all measurements of intensity, broadening, and position refer to the original scanned negative.

2.3. Wide-angle X-ray diffraction

X-ray studies of the black widow spider silk were performed at the microfocus beamline of the European Synchrotron Radiation Facility (ESRF) in Grenoble, France. Single strands of silk were aligned on a K-goniometer and the beam was focused to a spot size of 3 μm [10]. Diffraction patterns were recorded in scans across the fiber diameter, with steps of 1 μm in length; the beam was perpendicular to the fiber axis. Data were collected for 30 s per image, using a wavelength λ = 0.078 nm. Diffraction patterns were also recorded when the sample was displaced from the beam entirely, for later background subtraction measurements. An Al_2O_3 standard sample was examined for calibration purposes. The software package FIT2D was used for data reduction and peak profile fitting, with background subtraction [35].

The lattice parameters were calculated and the reflections indexed using the XFIX program contained in the CCP13 package [36]. Iterative calculations similar to those used in analysis of TEM SAD patterns were also performed. Crystal sizes were determined from diffracted beam spreading, using the Scherrer formula. As in TEM analysis, the degree of broadening was found by measuring the full-width half maximum (FWHM) of reflections along the radial direction.

2.4. Tensile testing

Rectangular supports were fashioned from thick, black paper, and a hole was cut through the center of each support with a standard UK hole punch (diameter 6 mm). A single *L. hesperus* dragline silk fiber was laid, straight but unstressed, across each hole, along the diameter parallel to the long direction of the support. Small drops of cyanoacrylate adhesive ('superglue') were used to attach the fiber to the card on either side of the hole. A minimum amount of glue was used in order to prevent it from wicking along the fiber length, so that the fiber would not be coated with glue to effectively produce a single-fiber composite. The silk fibers must be handled carefully in order to avoid premature stretching.

Prior to mechanical testing, fiber diameters were measured using an Olympus BX50 polarizing light microscope. A Micromat 200 Tensile Tester fitted with a 10 N load-cell was used for tensile tests. Fibers were loaded into the testing apparatus by securing the paper support between the grips. The sides of the support were then cut away carefully, so that all the force applied during the test would be carried by the fiber. An environmental chamber was used to control temperature and humidity. The tensile tests were performed at a strain rate of 10^{-4} s^{-1}, a temperature of 30 °C and a relative humidity of 60%.

3. Results and discussion

3.1. TEM polycrystalline diffraction

Longitudinal sections of *L. hesperus* silk fiber (Fig. 1) were used to obtain polycrystalline diffraction patterns exhibiting a

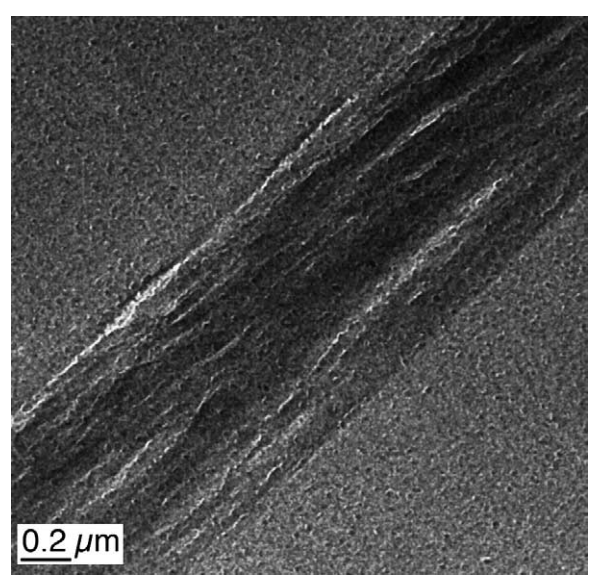

Fig. 1. Bright field TEM image of a longitudinal section of *L. hesperus* dragline silk, slightly defocused to optimize contrast. An aligned fibrillar substructure is evident.

fiber texture (Fig. 2). The texture shown in Fig. 2 indicates a preferred orientation of crystals, where the molecular backbone is aligned along the direction of the fiber axis. This crystal orientation was determined by comparing the alignment of the fiber in a bright field image with that of the diffraction pattern.

The diffraction patterns remain consistent along the length of the fiber, indicating that the crystals are widely and uniformly distributed and that the preferred orientation is preserved. The greatest fiber length sampled equaled 1 mm in these TEM specimens. Diffraction patterns from transverse cross-sectional specimens, where the incident beam is parallel to the fiber axis, did not show a preferred orientation. This observation indicates that the projection of the interchain and intersheet directions of the crystals onto the transverse cross-section are isotropically distributed in that plane.

The interchain and fiber axis lattice parameters have been shown to be conserved in a variety of spider and silkworm silks [33], and these values were confirmed by the electron diffraction patterns obtained in the present study. The intersheet distance, which is expected to vary from one silk to the next, was found to be equal to 10.8 Å. Thus, the lattice parameters for the *L. hesperus* orthogonal cell were confirmed (in the case of *a* and *b*) and found (in the case of *c*) to be: $a=$ 9.4 Å (interchain), $b=7.0$ Å (dipeptide, fiber axis), and $c=$ 10.8 Å (intersheet). A possible error of ± 0.02 nm is associated with the intersheet distance as determined here. Although it is common in polymer fiber diffraction studies to assign the unit cell *c*-axis to the chain direction, we have chosen to assign the unit cell *b*-axis to this direction. Our choice is motivated by the crystallographic convention that space group $P2_1$—which describes the unit cell symmetry of imperfectly crystalline NPL regions in spider dragline, where the screw axis lies parallel to the chains [12]—assigns the unique axis to be oriented along *b*.

The diffuse nature of the reflections qualitatively suggests that the crystals are small. The Scherrer formula was used to estimate the crystal dimensions from the arc width. The size of the crystals giving rise to fiber diffraction patterns, such as that shown in Fig. 2, was found to be ca. 2 nm. (A possible error of ± 1.0 nm, from the measurement of FWHM, is associated with this crystal size.) This value is consistent with a determination of crystal size from wide angle X-ray diffraction patterns, presented below.

When estimating the crystal size from the width of the diffraction arc, one must consider that the spreading of reflected beams does not necessarily arise from the small size

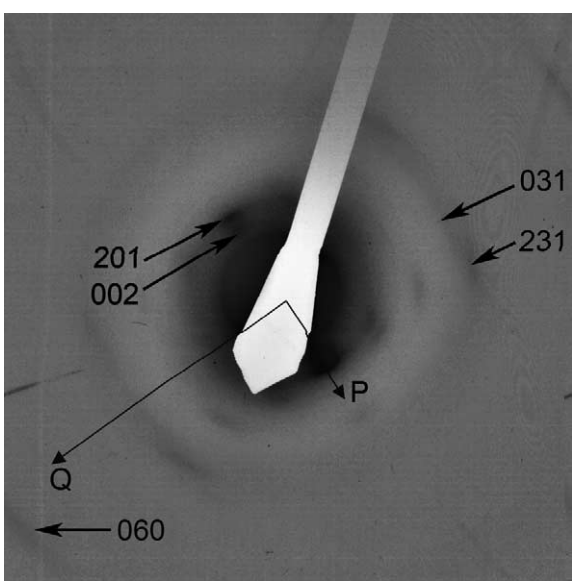

Fig. 2. Polycrystalline diffraction pattern, recorded from a longitudinal section of *L. hesperus* dragline silk. The pattern exhibits a fiber texture. Crystals giving rise to this diffraction pattern are aligned in a preferred orientation in which the molecular backbone is approximately parallel to the fiber axis. The proximity of *d*-spacings for (102) and (201) planes, equal to 0.47 and 0.43 nm, respectively, causes some uncertainty in the indexing of the 201 reflection. The 201 indices provided the closest match, however. Vectors *P* and *Q*, respectively, identify directions along which the spread of reflections 002 and 060 are measured in Fig. 3.

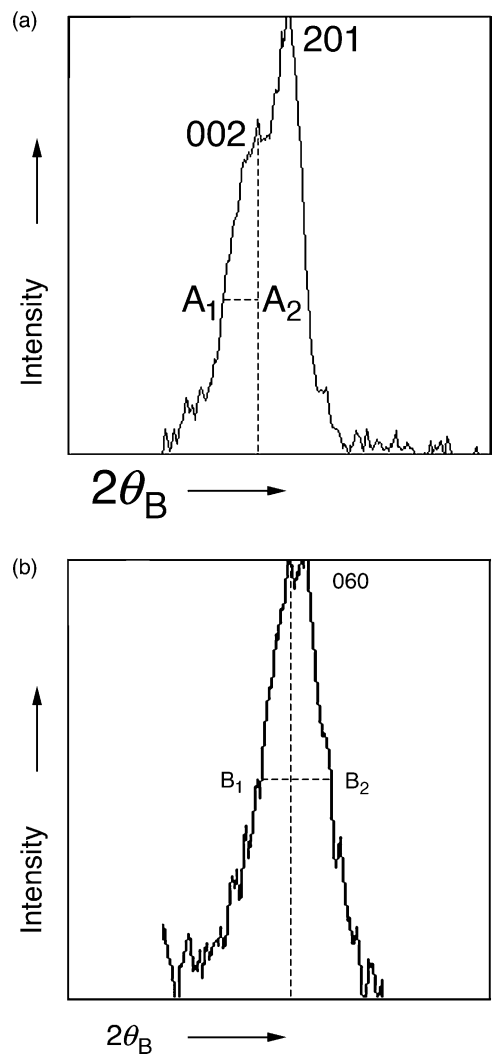

Fig. 3. (a) Plot used to measure the FWHM of the 002 peak from *L. hesperus* dragline silk. Because the 002 and 201 peaks overlap, the measured angular spread A_1A_2 was treated as a half-width and multiplied by two. For 002, $\theta_B=$ 0.0015 rad, $B=9.2\times10^{-4}$ rad, yielding $t_{001}=1.6$ nm; (b) Plot used to measure the FWHM (angular spread B_1B_2) of the 060 reflection from *L. hesperus* dragline silk. For 060, $\theta_B=0.0070$ rad, $B=7.6\times10^{-4}$ rad, yielding $t_{010}=$ 1.9 nm.

of crystals. Variations in lattice parameters can also contribute to the broadening of diffracted beams. In these β-sheet crystals, however, the nature of the bonds along the three crystallographic axes indicates that the lattice parameters should not vary in all three of these directions. Only the intersheet spacing should change significantly, if required to accommodate a variety of side-chains, while the interchain and dipeptide spacings should remain nearly constant. The broadening of the (060) reflection, in the fiber axis direction, revealed a crystal size that is of the same magnitude as the crystal size calculated from the broadening of the (002) reflection, in the intersheet direction (Fig. 3). This observation suggests that the primary reason for the beam broadening is not lattice parameter variations.

The fiber diffraction pattern is formed by many crystals; the ca. 2 nm crystal size reported above is averaged over a surface area of approximately 7 μm^2, defined by the SAD aperture. This crystal size does not necessarily represent the mean crystal size, however, since sharper reflections from larger crystals may be masked. As presented below, single crystal diffraction patterns were recorded from crystals that are more than 10 times larger than those characterized in the polycrystalline patterns. Diffraction spots from these larger crystals (ca. 40–120 nm in diameter) are sometimes visible in the background of the fiber texture diffraction patterns (Fig. 4). Diffraction from intermediate-sized crystals was not seen in any of our experiments, but could be hidden behind diffuse reflections in the fiber texture diffraction pattern. However, collective evidence, including a consideration of tensile properties as discussed below, supports a bimodal distribution of crystal sizes—rather than a continuum.

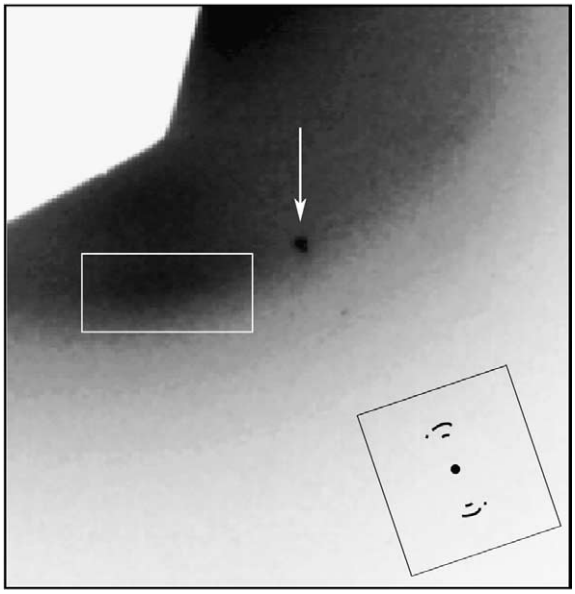

Fig. 4. Diffraction pattern recorded from a longitudinal section of *L. hesperus* dragline silk. The diffraction spot indicated by the arrow is displaced from the corresponding polycrystalline diffraction arc (inside the white box) by approximately 5–10°. Due to the faintness of the arc, a more accurate measurement is not obtainable.

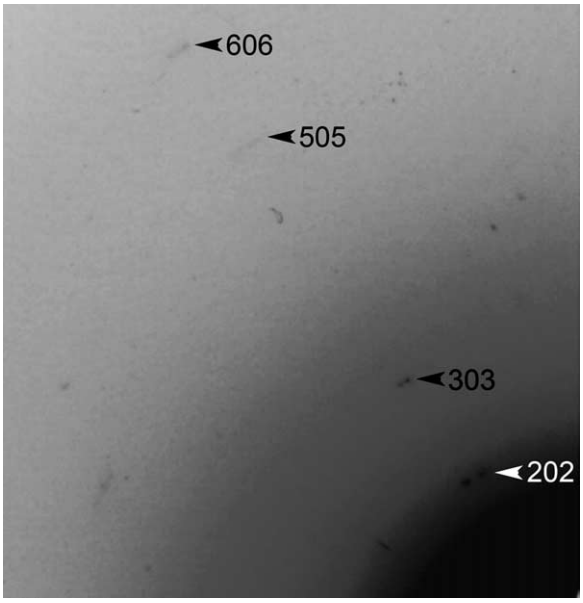

Fig. 5. Diffraction pattern recorded from a longitudinal section of *L. hesperus* silk. A zone axis could not be determined because only one vector is resolvable.

The ca. 2 nm sized crystals detected in polycrystalline diffraction patterns were not observed in bright and dark field images. Their size is close to the 1 nm resolution limit of the microscope used, and the 60–90 nm sample thickness would make it difficult for multiple overlapping crystals to be distinguished from the background.

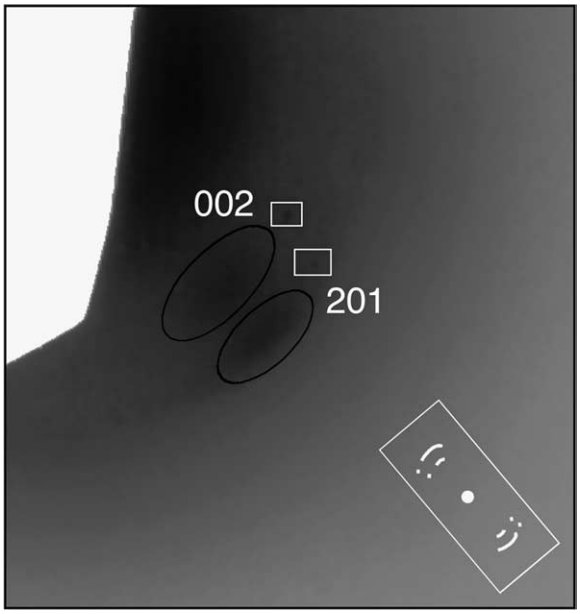

Fig. 6. Diffraction pattern recorded from a longitudinal section of *L. hesperus* dragline silk. Two single-crystal diffraction spots are enclosed in the white rectangles; corresponding polycrystalline arcs are enclosed in the dark ovals. The 002 single-crystal reflection (from a crystal of approximately 100 nm in diameter) is displaced by approximately $10 \pm 1°$ from the azimuthal spread of the 002 polycrystalline arc (from crystals of approximately 2 nm in diameter). The 201 single-crystal reflection is displaced by approximately $5 \pm 1°$ from the 201 polycrystalline arc. Angles are measured with respect to the origin.

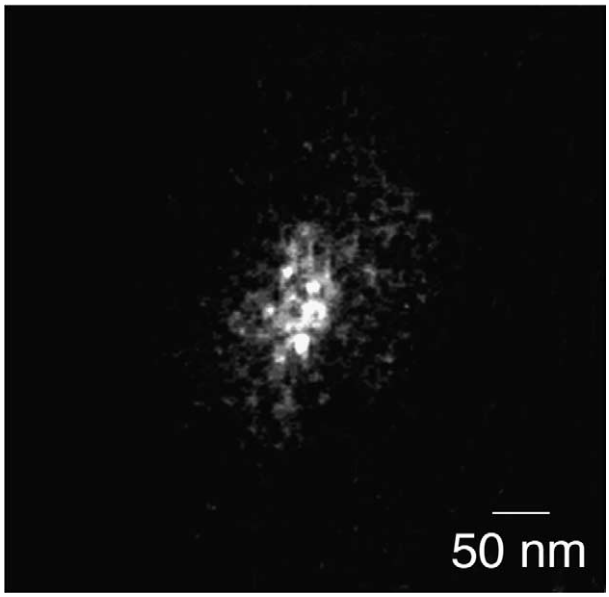

Fig. 7. Dark field TEM image of *Latrodectus hesperus* dragline silk, showing evidence of a crystal with approximate dimensions of 60×120 nm (±20 nm).

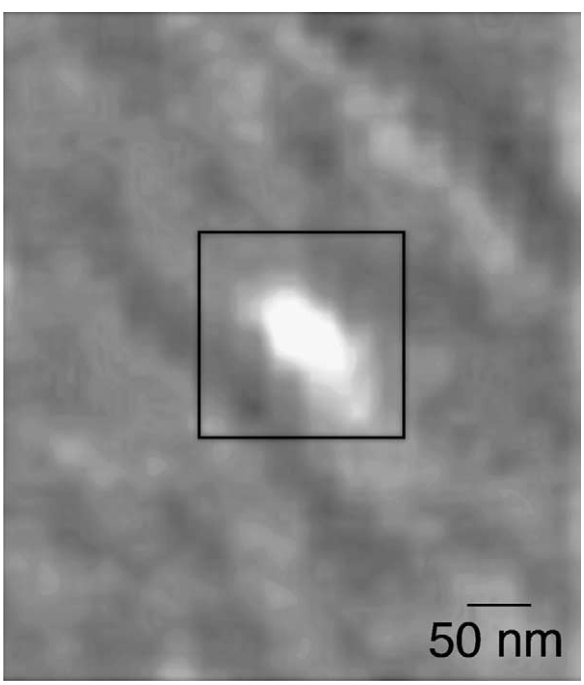

Fig. 8. Bright field TEM image of *L. hesperus* dragline silk, showing evidence (inside the black square) of a crystal with approximate dimensions of 50×100 nm (±20 nm). This contrast feature differs in appearance from other distinguishable contrast features observed in bright field images, including ice crystals and other extraneous material embedded in or on the silk. In the present case, the sample had been stained with a heavy metal to enhance the scattering by less ordered regions in the microstructure [13], which therefore appear darker than the crystal in bright field conditions. The immersion steps of the staining procedure were: (1) H_2O, 6 min; (2) aqueous solution with 0.5% uranyl acetate, 1.5 h, 40 °C, pH 4; (3) H_2O, 30 s; (4) aqueous solution with 2.7% lead citrate, 10 min, 20 °C, pH 11; (5) H_2O, 30 s.

3.2. TEM single crystal diffraction

Single crystal diffraction patterns were recorded from longitudinal cross-sections. These diffraction patterns consist of faint (low contrast) but sharp spots and streaks (Figs. 4–6), often originating from two or more crystals. The sharpness of the spots, as compared to the arcs in the polycrystalline pattern of Fig. 2, indicates that the single crystal patterns are generated by crystals significantly larger than the 2 nm crystal size derived from arc patterns. The breadth of the diffraction spots indicates that these crystals are approximately 20 times larger than the 2 nm sized crystals detected in polycrystalline patterns. The Scherrer formula was used to determine an approximate crystal size of 40 nm. (A possible error of ± 10 nm, from the measurement of reflection breadth, is associated with the determination of this crystal size.) TEM dark-field and bright-field images were recorded, which indicate crystals of approximately 40 nm in width and 120 nm in length (e.g. Figs. 7 and 8).

It was possible to index single crystal diffraction patterns, e.g. Fig. 5, using the lattice parameters determined from the polycrystalline diffraction patterns (smaller crystals). The streaking in some single crystal diffraction patterns (Figs. 5, 9 and 10) suggested lattice strains, consistent with the NPL model [11–13] of larger crystals in spider dragline. These strains are likely to occur in the intersheet direction, where the distance is governed by van der Waals packing of side chain moieties, and where packing of the β-sheets will vary depending on the amino acid side groups present. The presence of lattice strains in these larger crystals and their absence in the small 2 nm crystals is not surprising. In the case of a small crystal (high surface-to-volume ratio), the total volume free energy of formation is proportionately small, and thus would be insufficient to offset both a relatively high surface energy cost and a strain energy cost; small crystals with a side-chain composition that imposes lattice strains will simply not form.

Diffraction patterns indicate that the chain axis within the larger crystals is less strictly aligned with the fiber axis than that of the smaller crystals. This relationship was determined by comparing the alignment of the single crystal diffraction patterns to the orientation of the fiber as recorded in bright field images. In addition, a comparison of the respective alignment of small and large crystals is possible in diffraction patterns containing both arcs and spots, where diffraction spots are angularly displaced from the azimuthal spread of the arcs by 5–10° (Figs. 4 and 6). Small variations in the alignment of the larger crystals, with respect to one another, were also observed where diffraction from two or more crystals is visible on the same negative (Figs. 11 and 12).

3.3. Wide angle X-ray diffraction

The X-ray diffraction patterns contain Bragg reflections, a diffuse background, and an amorphous halo, as seen in previous studies of silk fibers using XRD [9,10] (Fig. 13). X-ray diffraction results confirmed the lattice parameters determined from TEM diffraction patterns, of: $a = 9.4$ Å

(interchain), $b = 7.0$ Å (dipeptide, fiber axis), and $c = 10.8$ Å (intersheet). (A possible error of ± 0.02 nm is associated with the intersheet distance as determined here.)

The measured breadth of reflections and the Scherrer formula were used to determine an average crystal diameter of 3.5 nm, with an associated error of ± 1.0 nm due to the measurement of FWHM. This value is in the same range as that

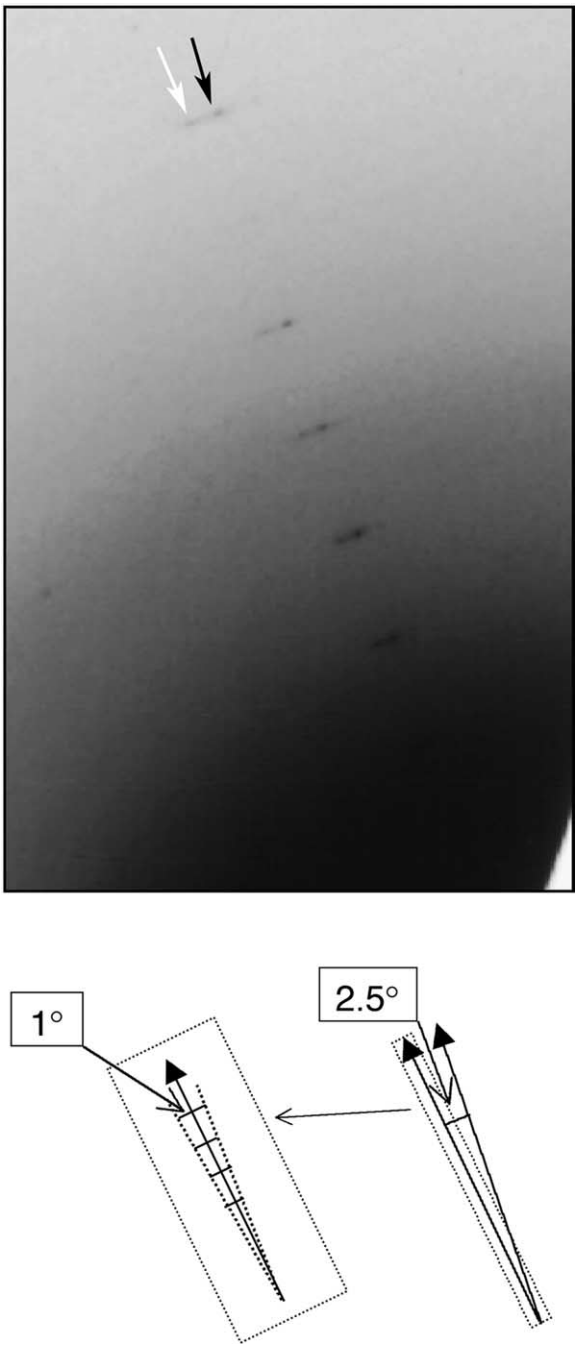

Fig. 9. Diffraction pattern recorded from a longitudinal section of *L. hesperus* dragline silk. Two sets of spots, indicated by the white and black arrows, are visible. Two vectors extend from the origin, one through each set of spots, separated by an angle of $2.5 \pm 0.5°$. Upon close examination, it is apparent that the set of spots indicated by a white arrow is composed of streaks, extending $1 \pm 0.5°$ azimuthally, i.e. along the circumference of a circle centred at the origin.

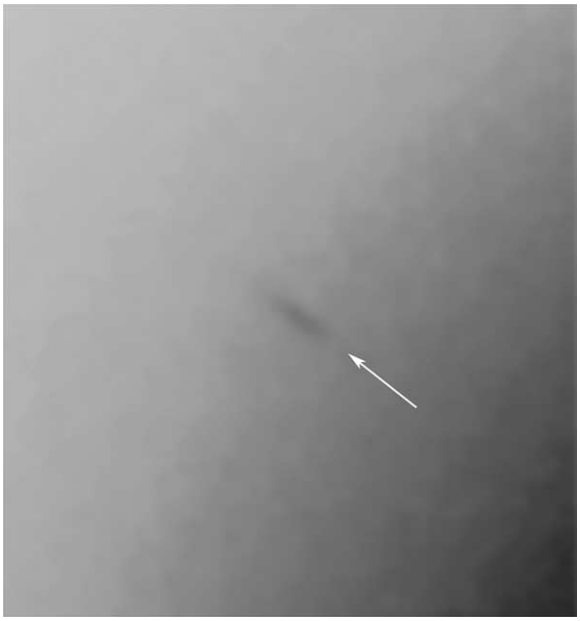

Fig. 10. Magnified region of a diffraction pattern recorded from a longitudinal section of *L. hesperus* dragline silk. The arrow points to a streak that extends along a vector from the origin. This streak indicates a change in lattice parameter (Δd) of 0.018 ± 0.010 nm.

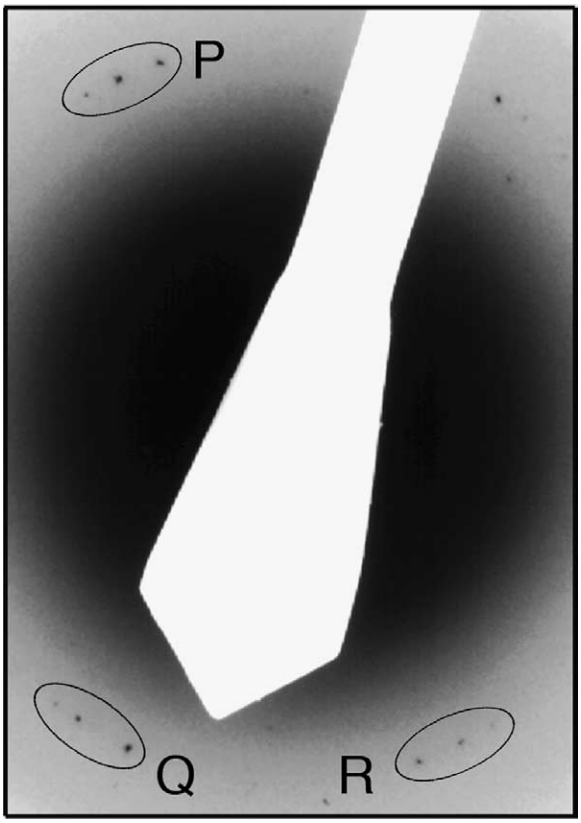

Fig. 11. Diffraction by single crystals recorded from a longitudinal section of *L. hesperus* dragline silk. Each of the ovals P, Q and R encloses three diffraction spots. The left and centre spots in group P are separated azimuthally by an angle of $5 \pm 0.5°$. The right and centre spots are separated by $7 \pm 0.5°$. Groups P, Q and R are related by symmetry.

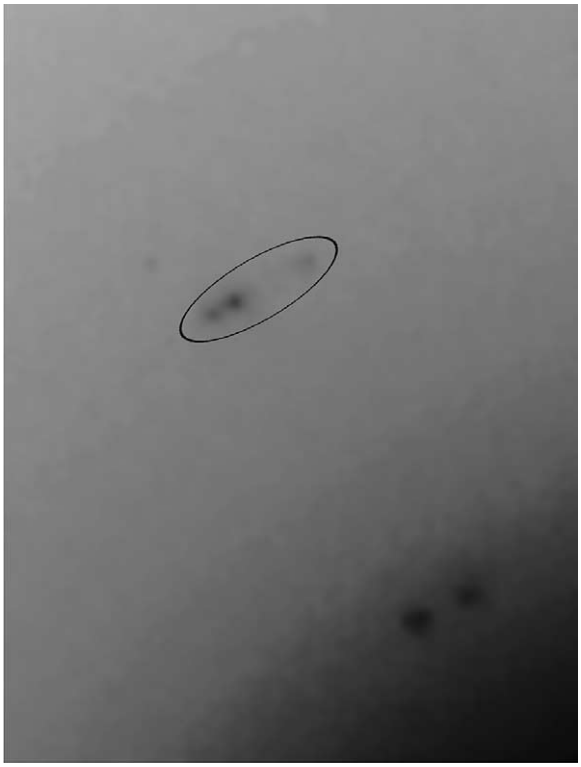

Fig. 12. Magnified region of a diffraction pattern recorded from a longitudinal section of *L. hesperus* dragline silk. The dark oval encloses three spots from different single crystals. The right and centre spots are separated azimuthally by an angle of $3 \pm 0.5°$. The left and centre spots are separated by an angle of $1 \pm 0.5°$.

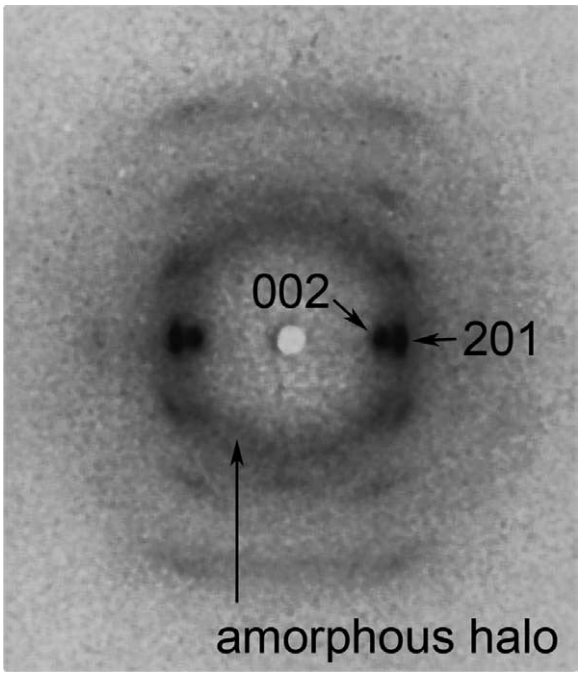

Fig. 13. X-ray diffraction pattern recorded from *L. hesperus* dragline silk. The fiber axis is vertical.

determined from TEM fiber diffraction patterns (2 nm $\pm$ 1.0 nm), and is also consistent with the results of previous XRD studies (2–7 nm) on silk fiber bundles [9] and single silk fibers [10] from spiders other than *L. hesperus*.

XRD did not provide evidence of the larger crystals (diameter ca. 40–120 nm) identified in TEM diffraction patterns. For the case of large crystals that have a chain axis orientation lying within the orientation range populated by the small crystals, the diffraction maxima will be masked by the (broader) maxima of the small crystals. For the case of large crystals with an orientation lying outside the range populated by the small crystals, the diffraction will be masked by background noise: individual crystals scatter weakly, as was already apparent in the diffraction patterns obtained by TEM, and the volume of material contributing to the background is greater in the case of XRD.

We considered the possibility that the larger crystals detected in the TEM might be the result of crystallization occurring at the cryogenic temperature at which the sample stage is maintained. However, we cannot reconcile the necessary scale of microstructural rearrangement with the extremely limited mobility of large protein chains in the solid state at and below room temperature.

3.4. Tensile testing

Examination in a light microscope revealed the fibrillar nature of the samples. The tensile tests were performed on fibrils that remained intact along their length, i.e. did not split into smaller fibrils. Results from tensile testing of single *L. hesperus* silk strands are shown in Table 1. The inter-sample variability is consistent with that observed in tensile tests performed on dragline from other spider species [37,38] and is indicative of the range of properties to which a spider potentially has access when it chooses to exercise control over the spinning process. The nanostructural origins of the high values of mean initial stiffness, breaking strength, and breaking strain (which collectively act to impart a high value of mean toughness) will be considered in Section 3.5.

3.5. Relating nanostructure to tensile properties

The TEM and X-ray diffraction results indicate the presence of crystals ca. 2 and 40–120 nm in size dispersed in an amorphous/semi-amorphous matrix. Both TEM diffraction and XRD confirm the presence of the smaller crystals, while only TEM diffraction showed evidence of the larger crystals. The

Table 1
Results of tensile tests performed on *Latrodectus hesperus* dragline silk

Sample	Young's modulus (GPa)	Breaking stress (GPa)	Breaking strain
1	25.23	1.766	0.150
2	28.84	2.331	0.129
3	18.91	0.802	0.110
4	19.11	1.698	0.143
Mean	23.02	1.649	0.133

crystal sizes reported here are upper and lower limits, and we cannot automatically discount the possibility that a range of crystal sizes exists in between these values. Diffraction from intermediate-sized crystals, which is less diffuse than that from smaller crystals, could be hidden under the reflections from smaller crystals in the polycrystalline patterns. The existence of two distinct crystal populations, one in the 2 nm range (well-oriented) and one in the 40–120 nm range (chain axis less strictly oriented with respect to the fiber axis), is supported by TEM diffraction patterns in which arcs from the smaller crystals coexist with spots from the larger crystals that are displaced from the arcs (Fig. 4).

A bimodal crystal size distribution, with small perfect polyalanine crystals and larger imperfect crystals incorporating glycine, alanine, and possibly other, larger, residues, is suggested by NMR results that indicate 40% highly oriented alanines, and 60% less well oriented alanines (to within ca. $\pm 60°$ of the fiber axis) in *N. clavipes* dragline silk [39]. This proposition is also consistent with NMR studies of the dragline silk of *N. edulis* spiders, that point to some of the glycine residues being partially aligned with respect to the fiber axis and likely incorporated into the β-sheet structure [14].

We can now consider how the force-elongation behavior of spider dragline might relate to a nanostructure in which there is a bimodal crystal size distribution. Termonia [40] published a two-dimensional model simulating the deformation and breaking of bonds in dragline, from the unstressed state to fracture. The model accounted for entanglements and hydrogen bonds within the amorphous matrix, β-sheet crystals, and a boundary layer between amorphous and crystalline regions. Stress–strain curves generated by Termonia's model for two different crystal sizes are reproduced in Fig. 14, with the horizontal axis re-scaled to display nominal strain rather than draw ratio. Both curves are for a volume fraction (V_c) of 0.45 and an amorphous/crystalline boundary layer of ca. 5 nm thickness (in the fiber axis direction). The case of small crystals (6×21 nm) predicts an elastic modulus of ca. 10 GPa and a tensile strength approaching 1 GPa. The case of large crystals (54×190 nm) predicts a higher elastic modulus (ca. 25 GPa) but a lower tensile strength (ca. 0.27 GPa). While the large crystals lead to high initial modulus values, they also create high local stress concentrations, which lead to failure of the sample at a relatively low strain.

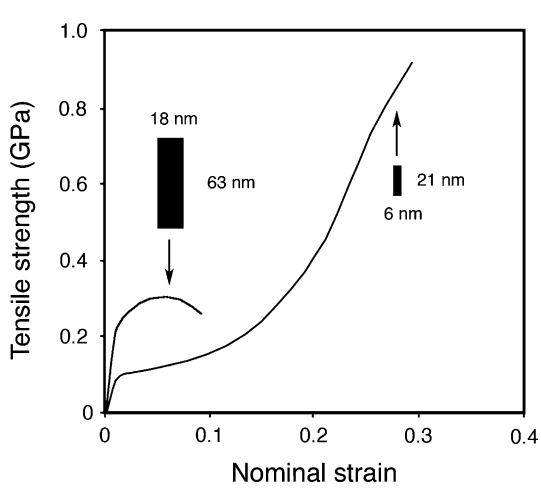

Fig. 14. Termonia's calculated stress–strain curves for small (ca. 6×21 nm) and large (ca. 18×63 nm) crystals (model is two-dimensional); figure adapted from Ref. [40].

The mean elastic modulus measured from *L. hesperus* dragline is 23 GPa—close to the 25 GPa theoretical modulus for the case of large crystals in Termonia's model. The tensile strength of *L. hesperus* dragline is ca. 1.7 GPa, closer to the case of small crystals in Termonia's model. A combination of the small and large crystals—as detected in TEM studies—could account for the force-elongation behavior of *L. hesperus* dragline silk.

Termonia's model assumes no breaking of crystallites. However, the larger crystals detected in *L. hesperus* dragline silk were found to be imperfect, as evidenced by lattice strains. Furthermore, they are less well oriented than the small crystals with respect to the fiber axis. These two factors mean that the larger, imperfect crystals may be able to deform plastically. Possible mechanisms are chain slip and eventual break-up of the crystals [41]. Larger crystals could thus confer a high initial elastic modulus and not act as stress centers past the yield point; thus, the plastic stage of the fiber deformation could be approximated by Termonia's stress–strain curve for the case of small crystals (Fig. 14). In the context of this simple model, the force-elongation behavior can therefore be thought of as dominated by the large crystal case during elastic deformation, and by the small crystal case subsequent to yield.

4. Conclusions

Results from TEM, XRD, and tensile mechanical testing of single dragline fibers from the cob-web weaver *L. hesperus* lead to the following conclusions:

(1) The orthogonal unit cell for crystalline regions in *L. hesperus* dragline silk is characterized by lattice parameters $a = 9.4$ Å (interchain), $b = 7.0$ Å (dipeptide, fiber axis) and $c = 10.8$ Å (intersheet).
(2) The TEM diffraction results provide the first explicit evidence of the co-existence of small and large crystals in a natural silk. Crystal sizes are on the order of 2 nm and 40–120 nm.
(3) The fine structure in single crystal electron diffraction patterns indicates the presence of lattice strains in the large crystals, suggesting that a variety of amino acid side groups are incorporated into these crystals. This observation is consistent with the NPL model of the larger crystals in *N. clavipes* dragline silk.
(4) The orientation distribution of the large crystals, as defined by the chain axis direction of crystals relative to the fiber axis, is broader than that of the small crystals.
(5) The force-elongation behavior of *L. hesperus* dragline is dominated by the large crystals during elastic (early-stage) deformation, and by the small crystals during plastic (late-stage) deformation.

Acknowledgements

We thank Joseph Spagna and Anne Moore (W.M. Keck Science Center, The Claremont Colleges, Claremont, CA) for providing *L. hesperus* dragline silk collected under controlled conditions. Cledwyn Merriman (Department of Plant Sciences, University of Oxford) assisted with TEM specimen preparation. Christian Riekel (European Synchrotron Radiation Facility, Grenoble) provided X-ray diffraction data and facilitated its analysis. David Cockayne (Department of Materials, University of Oxford) and John Gregg (Department of Physics, University of Oxford) contributed numerous helpful suggestions. Rafal Dunin-Borkowski (Department of Materials, University of Oxford) assisted with processing digital TEM images. J.E.T. was supported by a Rhodes Scholarship and a National Science Foundation Graduate Fellowship.

References

[1] Craig CL. Annu Rev Entomol 1997;42:231–67.
[2] Bini E, Knight DP, Kaplan DL. J Mol Biol 2004;335:27–40.
[3] Bell FI, McEwen IJ, Viney C. Nature 2002;416:37.
[4] Smith C, Ritchie J, Bell FI, McEwen IJ, Viney C. J Arachnol 2003;31:421–4.
[5] Viney C, Bell FI. Curr Opin Solid State Mater Sci 2004;8:165–71.
[6] Morrison NA, Bell FI, Beautrait A, Ritchie J, Smith C, McEwen IJ, et al. Mater Res Soc Symp Proc 2004;823:97–102.
[7] Haider M, Megeed Z, Ghandehari H. J Controlled Release 2004;95:1–26.
[8] Lazaris A, Arcidiacono S, Huang Y, Zhou J-F, Duguay F, Chretien N, et al. Science 2002;295:472–6.
[9] Grubb DT, Jelinski LW. Macromolecules 1997;30:2860–7.
[10] Riekel C, Branden C, Craig C, Ferrero C, Heidelbach F, Muller M. Int J Biol Macromol 1999;24:179–86.
[11] Thiel BL, Kunkel DD, Viney C. Biopolymers 1994;34:1089–97.
[12] Thiel BL, Guess KB, Viney C. Biopolymers 1997;41:703–19.
[13] Thiel BL, Viney C. J Microsc 1997;185:179–87.
[14] van Beek JD, Hess S, Vollrath F, Meier BH. PNAS 2002;99:10266–71.
[15] Trancik JE, Czernuszka JT, Cockayne DJH, Viney C. Polymer 2005;46:5225–31.
[16] Riekel C. Rep Prog Phys 2000;63:233–62.
[17] Thiel BL. The hierarchical structure of spider (major ampullate) silk. University of Washington, Seattle, WA. PhD Dissertation; 1995. [Copies available from University Microfilms, 1490 Eisenhower Place, P.O. Box 975, Ann Arbor, Michigan 48106].
[18] Barghout JYJ, Thiel BL, Viney C. Int J Biol Macromol 1999;24:211–7.
[19] Barghout JYJ, Czernuszka JT, Viney C. Polymer 2001;42:5797–800.
[20] Coddington JA, Chanzy HD, Jackson CL, Raty G, Gardner KH. Biomacromolecules 2002;3:5–8.
[21] Shen Y, Johnson MJ, Martin DC. Macromolecules 1998;31:8857–64.
[22] Trancik JE. Silk microstructures. University of Oxford, DPhil Thesis; 2000. [Copies available from Customer Services, The British Library, Document Supply, Boston Spa, Wetherby, West Yorkshire LS23 7BQ, UK. E-mail: dsc-customer-services@bl.uk].
[23] Guess KB. Effect of spinning rate on properties of major ampullate silk. University of Washington, Seattle, WA. MSE Thesis; 1995. [Copies available from University Microfilms, 1490 Eisenhower Place, P.O. Box 975, Ann Arbor, Michigan 48106].
[24] Guess KB, Viney C. Thermochim Acta 1998;315:61–6.
[25] Work RW. Textile Res J 1976;46:485–92.
[26] Vollrath F. ACS Symp Ser 1994;544:17–28.
[27] Elices M, Pérez-Rigueiro J, Plaza G, Guinea GV. J Appl Polym Sci 2004;92:3537–41.
[28] Ortlepp CS, Gosline JM. Biomacromolecules 2004;5:727–31.
[29] Trancik J, Czernuszka JT, Merriman C, Viney C. J Microsc 2001;203:235–8.
[30] Luft JH. J Biophys Biochem Cytol 1961;9:409–14.
[31] Causton B. Microsc Anal 1988;January:19–21.
[32] Wrigley NG, Brown E, Chillingworth RK. J Microsc 1993;130:225–32.
[33] Warwicker JO. J Mol Biol 1960;2:350–62.
[34] Cullity BD. Elements of X-ray diffraction. Reading, MA: Addison-Wesley Publishing Company, Inc.; 1978.
[35] Hammersley A. FIT2D; 1987. http://www.esrf.fr/computing/scientific/FIT2D/
[36] Denny R, Shotton M. XFIX: preliminary analysis of fiber diffraction patterns. UK: Daresbury Laboratory; 1998.
[37] Dunaway DL, Thiel BL, Viney C. J Appl Polym Sci 1995;58:675–83.
[38] Pérez-Rigueiro J, Elices M, Llorca J, Viney C. J Appl Polym Sci 2001;82:2245–51.
[39] Simmons AH, Michal CA, Jelinski LW. Science 1996;271:84–7.
[40] Termonia Y. Macromolecules 1994;27:7378–81.
[41] Kinloch AJ, Young RJ. Fracture behavior of polymers. London: Elsevier Applied Science Publishers Ltd; 1983.